Extreme- and high-synchrotron-peaked blazars at the limit of Fermi-LAT detectability: The γ -ray spectrum of 1BIGB sources

MNRAS 000, 1–13 (2018) Preprint 26 April 2018 Compiled using MNRAS LATEX style file v3.0

Extreme & High Synchrotron Peaked Blazars at the limit of *Fermi*-LAT detectability: the γ-ray spectrum of 1BIGB sources

B. Arsioli[1,2,5]★, U. Barres de Almeida[3,5]†, E. Prandini[4]‡, B. Fraga[3,5], L. Foffano[4],
[1]*Instituto de Física Gleb Wataghin, Universidade Estadual de Campinas (UNICAMP), Rua Sérgio Buarque de Holanda 777, 13083-859 Campinas, Brazil*
[2]*Science Data Center della Agencia Spaziale Italiana, SSDC - ASI, Rome, Italy*
[3]*Centro Brasileiro de Pesquisas Físicas (CBPF), Rua Dr. Xavier Sigaud 150, 22290-180 URCA, Rio de Janeiro, Brasil*
[4]*University of Padova, Department of Physics and Astronomy, and INFN sez. Padova, Italy*
[5]*ICRANet-Rio, CBPF, Rua Dr. Xavier Sigaud 150, 22290-180 URCA, Rio de Janeiro, Brazil*

Received: April 23, 2018

ABSTRACT

We present the 1-100 GeV spectral energy distribution for a population of 148 high-synchrotron-peaked blazars (HSPs) recently detected with *Fermi*-LAT as part of the First Brazil-ICRANet Gamma-ray Blazar catalogue (1BIGB). Most of the 1BIGB sources do not appear in previous *Fermi*-LAT catalogues and their γ-ray spectral properties are presented here for the first time, representing a significant new extension of the γ-ray blazar population. Since our sample was originally selected from an excess signal in the 0.3 - 500 GeV band, the sources stand out as promising TeV blazar candidates, potentially in reach of the forthcoming very-high-energy (VHE) γ-ray observatory, CTA. The flux estimates presented here are derived considering PASS8 data, integrating over more than 9 years of *Fermi*-LAT observations. We also review the full broadband fit between 0.3-500 GeV presented in the original 1BIGB paper for all sources, updating the power-law parameters with currently available *Fermi*-LAT dataset. The importance of these sources in the context of VHE population studies with both current instruments and the future CTA is evaluated. To do so, we select a subsample of 1BIGB sources and extrapolate their γ-ray SEDs to the highest energies, properly accounting for absorption due to the extragalactic background light. We compare those extrapolations to the published CTA sensitivity curves and estimate their detectability by CTA. Two notable sources from our sample, namely 1BIGB J224910.6-130002 and 1BIGB J194356.2+211821, are discussed in greater detail. All γ-ray SEDs, which are shown here for the first time, are made publicly available via the Brazilian Science Data Center (BSDC) service, maintained at CBPF, in Rio de Janeiro.

Key words: active galactic nuclei – blazars – gamma rays – very high-energy

1 INTRODUCTION

The *Fermi*-LAT sources and specially the high-energy catalogues, 2FHL (50 GeV, Ackermann et al. 2016) and 3FHL (10 GeV, Ajello et al. 2017), provide the best unbiased proxy to the very-high-energy (VHE) extragalactic sky. Meaningful extrapolations can be derived therefrom, as to what are the expectations for future studies in this extreme observational window.

Complementary to those works is the 1BIGB catalogue (Arsioli & Chang 2017), which contains 150 extragalactic γ-ray sources associated to excess signals $> 3\sigma$ in the 0.3-500 GeV band as observed with *Fermi*-LAT. Bearing nearly no overlap with the previous *Fermi*-LAT catalogues, the 1BIGB presents sources which were found through targeted analysis of a group of candidate VHE blazars obtained from the 1WHSP and 2WHSP catalogues (Arsioli et al. (2015) and Chang et al. (2017)), selected on the basis of their IR and X-ray spectral energy distribution (SED) synchrotron properties. Collectively, the objects in the 1BIGB catalogue represent a unique sample from a population of extragalactic objects at the limit of *Fermi*-LAT detectability, and which are at the extreme of blazar phenomenology.

Blazars are active galactic nuclei believed to produce γ rays inside relativistic jets which beam the emission towards the observer with bulk Lorentz factors of ~ 10 or larger (Urry & Padovani 1995). The γ-ray production mechanism in blazars is not completely understood, evidence suggesting that most of the emission has a leptonic origin, although a significant but yet unquantified contribution from hadronic processes cannot be excluded (Cerruti et al. 2017). Good sampling of the γ-ray SED of these objects is therefore fundamental for blazar studies (Böttcher et al. 2013). A related example is the recent effort to unveil new γ-ray Low-

★ E-mail: arsioli@ifi.unicamp.br, bruno.arsioli@ssdc.asi.it
† E-mail: ulisses@cbpf.br
‡ E-mail: prandini@pd.infn.it

Synchrotron-Peaked (LSP) blazars (Arsioli & Polenta 2018), previously expected to be γ-ray quiet.

The SEDs from blazars can extend along many decades in energy, from a few GHz in radio, up to TeV γ rays, and are usually characterized by the presence of a synchrotron and an inverse-Compton (IC) bumps in the Log (ν) vs. Log (νf_ν) plane (Padovani et al. 2017). The peak-power associated to the synchrotron bump tells us at which frequency most of the AGN electromagnetic power is being released, the parameter Log (ν^{syn}_{peak}) being extensively used to classify blazars. Following discussions from Padovani & Giommi (1995), Abdo et al. (2010b) and Ghisellini (1999), objects with Log(ν^{syn}_{peak}) < 14.5, in between 14.5 to 15.0, and > 15.0 [Hz] have been called, respectively, low-, intermediate-, and high-synchrotron-peak blazars (LSP - ISP - HSP).

Recent observational data in hard X-rays (Costamante et al. 2017) support the existence of a population of extreme high-energy synchrotron peaked sources (EHSPs). The class had been first proposed by Costamante & Ghisellini (2002), being composed of sources with a synchrotron peak frequency above 10^{17} Hz. Clear indications or evidence for the synchrotron peak actually reaching the MeV range is nevertheless still under debate, as in the following works: Chang et al. (2017); Tanaka et al. (2014a); Kaufmann et al. (2011); Tavecchio et al. (2011).

Extreme HSPs are characterized by low luminosity and limited variability, in contrast to typical HSP blazars; the weak variability, however, could be biased by the limited sensitivity of current instruments, rather than to intrinsic characteristics of the sources. The high synchrotron peak (and consequently high IC peak) and low luminosity of EHSPs seem to support the blazar sequence paradigm (Fossati et al. 1998; Ghisellini et al. 2017). However, the expected shift of both SED peaks to higher energies has not been firmly established yet. We should also call attention to the fact that nearly half of the 1BIGB sources (63 objects) have no measured redshift and another 21 only have an estimated lower-limit redshift. Therefore, as typical of HSP blazars, many 1BIGB sources have no derived luminosity, which could introduce strong bias to the blazar sequence paradigm, as extensively discussed in Arsioli et al. (2015) with focus to HSP blazars.

Since EHSPs are possibly characterized by an IC peak at VHE γ rays, they are not easy to observe, being hardly detected in current γ surveys as well. For example, one of the brightest such sources in X-rays, and the best-studied extreme blazar to date, 1ES 0229+200, was detected by *Fermi*-LAT only in the 3FGL, after 4 years of exposure. The HE and VHE γ-ray spectra for this object were shown to connect smoothly and to be very hard, with no apparent break up to TeV energies (Aharonian et al. 2007).

EHSPs draw increasing attention given the possibility that blazars might be associated to astrophysical neutrinos (Padovani et al. 2016, 2018), and ultra-high-energy cosmic rays (Resconi et al. 2017). Extreme blazars have also large impact as probes of the extragalactic background light (EBL) and cosmic magnetic fields (Bonnoli et al. 2015). Given the broad context in which blazars play an important role in future astro-particle physics, describing new γ-ray spectral properties of HSP and EHSP-candidates becomes of major relevance.

An unbiased population study of blazars at VHE γ rays is made difficult by the fact that these objects are characterised by intense flaring activity. In fact, many of the known VHE γ-ray blazars have been detected via triggers based on high states from other bands, rather than through surveys. To produce good estimates on the size and nature of the blazar population potentially detectable at VHEs is therefore an important task. Furthermore, completing the information available on the faint and extreme sector of blazar phenomenology is specially useful, with implications for the determination of their luminosity function (the log N − log S distribution), and the estimates of the total γ-ray background (Inoue & Ioka 2012; Ackermann et al. 2015).

Observations with the current class of VHE instruments, as well as *Fermi*-LAT (Tanaka et al. 2014a), seem to corroborate with the existence of a population of EHSPs with IC peak above 100 GeV in the γ-ray band. *Fermi*-LAT, for which sensitivity is already greatly decreasing above 100 GeV, might nevertheless be probing only the low-energy side of the IC component, which could easily reach beyond the TeV range. As a result, these putative EHSPs are clearly undersampled in current *Fermi*-LAT catalogues, with just three well-studied sources in the local universe up to date – Mkn 421 and Mkn 501 (at $z \sim 0.03$) and 1ES 0229+200 (at $z = 0.14$).

By virtue of its selection methodology, the blazar population in the 1BIGB catalogue is composed of faint HSP blazars and extreme blazars. Until now, a source-by-source discrimination between the two classes has not yet been possible though, due to the limited information available on the synchrotron SED and on the 0.3-500 GeV γ-ray excess. The fact that most of the objects presented is this work do not show up in previous *Fermi*-LAT catalogues, points to a significant new extension of the blazar population, with important implications to the extragalactic science case of currently active VHE γ-ray observatories, as well as for the future Cherenkov Telescope Array, CTA (CTA Consortium et al. 2017; Sol et al. 2013).

In this work we analyze the complete sample of 1BIGB sources, using the latest PASS8 *Fermi*-LAT data release (Atwood et al. 2013), and present, for the first time, their 1-100 GeV γ-ray spectra. The final list results in the richest high-energy spectral sample of faint HSPs and candidate extreme blazars to date, providing useful new information for the classification of these objects, given that only low-energy SED information was previously available. As we discuss in following Section 5, the catalogue constitutes also a potential list of targets for current and future VHE observational programmes.

The paper is organised as follows. In Section 2, we describe in detail the 1BIGB sample and calculate updated 0.3-100 GeV broadband fitting for all sources, integrating over 9.3 yrs of currently available data. In Section 3 we present for the first time, the 1-100 GeV γ-ray SEDs of its 148 sources. In Section 4 we stack the γ-ray SEDs, providing a common view of the source population, discuss about the *Fermi*-LAT sensitivity limit at 10 GeV, and present two notable sources from our sample. Finally, in Section 5 we briefly compare our results to the published sensitivity curves of MAGIC, H.E.S.S., and CTA, in order to estimate the detectability and the impact of our source population to current and future VHE γ-ray studies.

2 THE 1BIGB SAMPLE DESCRIPTION

The 1BIGB sample was built based on the selection of 400 γ-ray candidates from the 1WHSP and 2WHSP samples. Those candidates comprise HSPs with the brightest synchrotron peaks Log (νf_ν) > -12.1 erg/cm^2/s, but having no counterpart in previous *Fermi*-LAT catalogues – 1FGL, 2FGL and 3FGL (Abdo et al. 2010a; Nolan et al. 2012; Acero et al. 2015). A likelihood analysis in the 0.3-500 GeV band, integrating over 7.2 years of *Fermi*-LAT observations, and using the PASS8 data release, unveiled a total

of 150 γ-ray signatures, of which 85 had high-significance, with Test Statistics (TS, Mattox et al. 1996) ranging from 25 up to 130 (all >5σ detections) and the remaining 65 had lower-significance, with TS in between 10 to 25 (3 to 5σ detections). Many low and high-significance detections were studied with the help of γ-ray TS maps, showing a typical point-like source emerging from a smooth background. In addition, the sample showed γ-ray spectral properties as expected for HSP blazars, with photon spectral index $\langle\Gamma\rangle \sim 1.94$. Given that each of those 150 signatures is associated to a powerful HSP counterpart, they represent robust detections at the edge of *Fermi*-LAT sensitivity (as well described by Figure 8 from Arsioli & Chang 2017), grouped under the acronym 1BIGB.

2.1 Updating the 1BIGB broadband fit between 0.3-500 GeV

The 1BIGB detections considered a broadband likelihood analysis between 0.3-500 GeV, integrating data from August 04 2008 up to November 04 2015 (~7.2 years). Since that time, *Fermi*-LAT has accumulated more than 2 additional years of observation time (at the time of writing, we have available data up to December 05 2017). Taking advantage of a larger exposure time with *Fermi*-LAT, we thus refine the power-law fitting for each 1BIGB source by performing a likelihood analysis similar to Arsioli & Chang (2017), applying the same setup and data quality cuts.

We update the 1BIGB power-law parameters and re-evaluate the TS values considering the current 9.3 years of observation, aiming to deliver the most significant description up to date. For this broadband analysis we integrate over the entire 0.3-500 GeV energy band, using PASS8 data release, and assuming that the γ-ray spectrum of each γ-ray source can be described by a power-law:

$$\frac{dN}{dE} = N_0 \left(\frac{E}{E_0}\right)^{-\Gamma} , \qquad (1)$$

where E_0 is a scale parameter (also known as pivot-energy), N_0 is the prefactor (normalization) corresponding to the flux density in units of ph/cm^2/s/MeV at the pivot energy E_0, and Γ is the photon spectral index for the energy range considered. Both Γ and N_0 are set as free parameters and further adjusted by the likelihood fitting routine. Source positions and $E_0 = 1000$ MeV are set as fixed parameters, kept constants for the analysis. In the source-input xml file, all sources within 10° from the candidate had both Γ and N_0 parameters flagged as free[1], and therefore their 3FGL models that are based on 4 years of observations will be adjusted. This particular choice increases the computational burden of the analysis, but is crucial for adapting the model maps to the extra 5.3 years of exposure being considered. A sub-sample of the results, listing only 13 cases detected with TS>100 is shown in Table 1; a list with the total 148 cases which had good convergence will be available as on-line material.

For most cases the Γ parameter estimates obtained by integrating over 7.2 ($\Gamma_{7.2}$) and 9.3 ($\Gamma_{9.3}$) years are relatively stable, since the intrinsic variability is well contained within the error bars (compared to the red-dashed line in Figure 1, for $\Gamma_{7.2} = \Gamma_{9.3}$). There were only two cases which did not show good likelihood-convergence when integrating along 9.3 yrs, namely 1BIGB J080135.8+463824 and 1BIGB J145508.2+192014, which were removed from the 1BIGB SED list. We would like to note that those sources had TS close to 10 in the previous 1BIGB sample (7.2 years). Few non-detections are expected when integrating over different time-windows, specially owing to the uncertainty induced by source variability.

[1] In this regard we are following recommendations from Fermi Science Tools user guide https://fermi.gsfc.nasa.gov/ssc/data/analysis/scitools/binned_likelihood_tutorial.html which advise users to set free parameters at least within 7° from the source of interest. This is a consequence of the large point spread function (PSF) specially at the low-energy threshold, which can overlap with nearby sources. Therefore, in order to get a confident description of a particular source, we need to properly fit and adjust the whole environment around it.

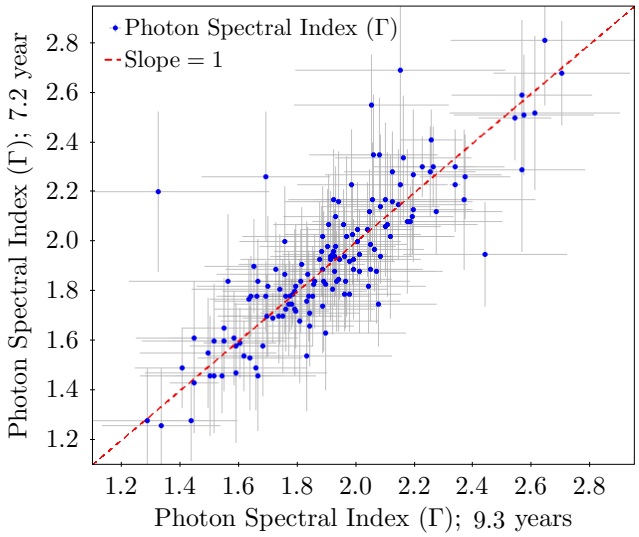

Figure 1. Comparison between the photon spectral index (Γ) integrating over for 7.2 years of exposure, with the updated values calculated with 9.3 years of observations with *Fermi*-LAT. The Γ factor considers a power-law fit to the entire 0.3-500 GeV energy band, and its corresponding error bars are represented in gray. The red-dashed line is a curve with slope equal one.

3 THE γ-RAY SPECTRAL ENERGY DISTRIBUTION

The 1BIGB sample is composed of γ-ray sources which are, on average, faint and close to the detectability limit of *Fermi*-LAT. In the process of building the γ-ray SEDs, we had to deal with the problem of poor photon counts when integrating over a short energy bin. In most cases, simply dividing the broadband energy (between 1 GeV and 500 GeV) in equally spaced logarithmic bins result in low TS detections per bin, which most of the times only become upper limits for the SED. This is the usual way SEDs are built, and inevitably a considerable amount of relevant information available via broadband analysis is not being incorporated.

In order to capture the shape of the γ-ray spectrum and estimate reliable SED data points, we integrate each energy bin over a large energy band (larger than 'equally spaced logarithmic bins') and evaluate the flux at a specific energy for each bin. In other words, we take into account information from a broadband analysis by accepting superposed energy channels.

Table 2 describes the energy bands over which we integrate in order to estimate fluxes at specific pivot-energies (E_0), later used to build the γ-ray SEDs. We choose those E_0 values to be close to equally spaced bins in Log(E) scale, with increments of the order of $\sim 10^{0.25}$. For example, starting from the 1 GeV SED point we integrate over 1.0 to 5.0 GeV, adjusting a power-law (see Equation (1))

Table 1. Table showing the model description for 13 of the 148 1BIGB γ-ray signatures, all detected with TS>100. Note that a complete table with all the 148 source is available on-line. The first three columns show respectively the 1BIGB source names, right ascension R.A. and declination Dec. in degrees (J2000). The fourth column shows the reported redshifts from literature (Shaw et al. 2013b; Pita et al. 2014; Furniss et al. 2013; Danforth et al. 2010; Shaw et al. 2013a; Masetti et al. 2013; Sbarufatti et al. 2005; Massaro et al. 2015). The flag ? is used for values reported as uncertain; lower limits are marked with ">" (all lower-limits shown here were derived in Arsioli et al. 2015; Chang et al. 2017), and sources with currently absent redshift were given 0. value. The γ-ray model parameters from the *Fermi* Science Tools assume a power-law to describe the spectrum within the studied energy range 0.3-500 GeV. The parameter N_0 (see Equation (1)) is given in units of ph/cm^2/s/MeV, and Γ is the spectral photon index, which are direct outputs from the likelihood analysis over 9.3 years of *Fermi*-LAT data in the 0.3-500 GeV band; those results consider the pivot energy fixed as $E_0 = 1$ GeV. The column Flux gives the photon counts in units of ph/cm^2/s calculated by integrating Equation (1) along the energy range 1-100 GeV, column E-Flux corresponds to the energy flux in units of MeV/cm^2/s. For the columns Flux and E-Flux, upper and lower case values represent positive and negative errors, respectively.

1BIGB Source name	R.A. (deg)	Dec. (deg)	z	Γ	N_0 (10^{-15})	TS	Flux$^{\times 10^{-10}}_{1-100\,GeV}$	E-Flux$^{\times 10^{-13}}_{1-100\,GeV}$
1BIGBJ021631.9+231449	34.13333	23.24722	0.288	1.88±0.10	2.49±0.52	116.4	$2.76^{0.98}_{-0.79}$	$15.0^{4.7}_{-3.3}$
1BIGBJ044240.6+614039	70.66917	61.6775	0.	2.01±0.09	4.00±0.71	145.0	$3.92^{1.12}_{-0.95}$	$17.9^{4.3}_{-3.2}$
1BIGBJ050335.3-111506	75.8975	-11.25167	>0.57	1.85±0.11	2.30±0.53	102.6	$2.63^{1.03}_{-0.82}$	$15.0^{5.1}_{-3.5}$
1BIGBJ050727.1-334635	76.86333	-33.77639	0.	1.79±0.11	1.84±0.43	125.0	$2.25^{0.93}_{-0.72}$	$14.1^{5.0}_{-3.5}$
1BIGBJ075936.1+132116	119.90042	13.35472	0.	1.75±0.09	2.12±0.44	152.6	$2.71^{0.98}_{-0.79}$	$17.9^{5.5}_{-4.0}$
1BIGBJ082904.7+175415	127.27	17.90417	0.089	2.25±0.10	4.47±0.55	136.8	$3.55^{0.79}_{-0.67}$	$12.1^{2.7}_{-2.0}$
1BIGBJ113755.6-171041	174.48167	-17.17833	0.6	1.71±0.10	1.90±0.43	126.9	$2.55^{1.00}_{-0.79}$	$18.0^{6.0}_{-4.2}$
1BIGBJ121510.9+073203	183.79542	7.53444	0.137	1.64±0.11	1.26±0.37	105.5	$1.87^{0.97}_{-0.72}$	$14.9^{6.2}_{-4.1}$
1BIGBJ144236.4-462300	220.65167	-46.38361	0.103	1.92±0.10	3.14±0.64	107.7	$3.33^{1.14}_{-0.93}$	$17.1^{5.0}_{-3.6}$
1BIGBJ154202.9-291509	235.5125	-29.2525	0.	1.78±0.08	2.62±0.50	143.2	$3.27^{1.04}_{-0.86}$	$20.8^{5.4}_{-4.1}$
1BIGBJ194356.2+211821	295.98417	21.30611	0.	1.44±0.08	2.01±0.57	194.7	$3.93^{1.84}_{-1.44}$	$42.9^{13.2}_{-9.8}$
1BIGBJ200204.0-573644	300.51708	-57.6125	0.	2.08±0.10	2.93±0.49	105.5	$2.69^{0.78}_{-0.64}$	$11.2^{3.0}_{-2.2}$
1BIGBJ224910.6-130002	342.29458	-13.00056	>0.5	2.33±0.01	87.01±1.43	11240.5	$64.8^{1.93}_{-1.88}$	$202.8^{6.2}_{-6.0}$

Table 2. Definition of energy bins used for the broadband analysis, to estimate fluxes N_0 at each pivot energy E_0. The estimate is done via likelihood analysis, adjusting a power-law to each energy bin.

E_0 [GeV]	Integrate over [GeV]
1.0	1.0 - 5.0
1.7	1.0 - 10.0
3.0	1.0 - 17.0
5.0	1.0 - 30.0
10.0	1.7 - 50.0
17.0	3.0 - 100.0
30.0	5.0 - 170.0
50.0	10.0 - 300.0
100.0	30.0 - 500.0

to this interval and setting $E_0 = 1$ GeV, so that N_0 represents the flux at 1 GeV when taking into account the spectral trend in the selected energy-bin. For the later SED point at 1.7 GeV, we increment the energy band by a factor $\sim 10^{0.25}$, therefore integrating over 1.0 to 10 GeV, so to capture the power-law trend when estimating an SED point at higher energy. We proceed in this way up to the 5 GeV SED point, and for the next ones we start incrementing both the low and high-energy band by a factor $\sim 10^{0.25}$, till we reach the 100 GeV SED data point, with a high-energy threshold of 500 GeV.

Considering the total of 1350 likelihood analysis (integrating over 9.3 yrs) needed to be computed for building the entire SED catalogue, we limit the low energy band to 1 GeV to improve the computation time. Given that the photon counts at 1 GeV and higher energy levels are relatively reduced with respect to lower energy bands, working with a cut at 1 GeV allows the likelihood to converge in a reasonable time (so that a large scale analysis could be performed). The cut in energy also adjusts well to the hard γ-ray spectral slope expected for HSP sources; taking into account that the detector PSF improves with increasing energy, the energy cut also helps to avoid contamination from nearby sources.

In the source-input xml file, all sources within 10° from the candidate are set free to vary their spectral fitting parameters, just as used in previous broadband analysis (Section 2.1). Both Γ and N_0 are set as free parameters and further adjusted by the `gtlike` fitting routine. The source position and the scaling E_0 are set as fixed parameters, with E_0 changing only according to the SED point being calculated. At this point, we call attention to the choice of the pivot-energy E_0, which corresponds to the energy where the differential flux N_0 [ph/MeV/cm^2/s] is going to be estimated. Later, we compute the flux [erg/cm^2/s] at a given E_0 simply converting[2]: flux = $N_0 \cdot E_0^2 \cdot 1.602\times10^{-6}$, and cases showing TS < 6.0 per bin are given upper limits. This is how we combine a broadband analysis with the flux calculation for each energy bin, to deal specifically with faint sources.

For the highest energy channels 50 GeV and 100 GeV, a broadband binned analysis suffers from rather low photon counts, to which an unbinned analysis is much better adapted. Therefore, for those two channels we have applied unbinned analyses, assuring a good SED agreement between the few 1BIGB sources which are

[2] The factor 1.602×10^{-6} is used to convert MeV to erg.

also part of the 2FHL and 3FHL catalogues. As an example[3] we cite the cases of 1BIGB J044240.6+614039, 1BIGB J030433.9-005403 and 1BIGB J113046.0-313807.

4 AVERAGE γ-RAY BEHAVIOR AND BLAZAR POPULATIONS

The 1BIGB catalogue contains average spectral information about the sources derived from a 0.3-500 GeV broadband analysis. With the purpose of investigating in more detail the spectral properties of these faint objects, here we present the 1-100 GeV spectral points resulting from the analysis of 9.3 years of *Fermi*-LAT data as reported in the previous Section. As can be seen in Figure 2, the spectral points populate the full energy window under consideration, except for the highest energy bin, around 100 GeV, where only 13% of the blazars present a significant signature.

When considering an individual power-law fit to the γ-ray spectrum, the derived photon spectral index covers a wide range from 1.26 to 2.81, with an average error on the slope of the order of 10%. The large spread in spectral slopes suggests that the objects composing this catalogue do not present any common spectral feature at the HE γ-ray band. No characteristic spectral turnover, nor spectral break, correlating with other properties such as synchrotron-peak frequency or flux level was found.

At first glance such results may look at odds with expectations from a description following the blazar sequence (Costamante et al. 2001); we remind, nevertheless, the fact that an effective population study is hardly possible here, given the limited sample size and the lack of homogeneity in the sample selection, which is composed of objects distinguished only by being at the very limit of *Fermi*-LAT detectability. The 1BIGB source population is therefore likely composed of a mixture of faint HSPs and extreme-HSP blazars.

Within the population, two sources stand out showing a γ-ray spectrum which clearly exceed most objects in flux. All the remaining sources are clustered in a region of νF_ν between 10^{-13} and 10^{-12} erg/cm^2/s, with no clear common spectral trend correlated to synchrotron peak information. The two peculiar sources will be further discussed in Section 4.3.

We fitted the clustered points for the remaining sources with a power-law (red line in Figure 2) and found an average photon spectrum slope of $\Gamma \sim 1.86$. This suggests that for the 1BIGB population as a whole, the peak of the second SED bump is located at energies larger than those covered by our analysis, falling within the VHE γ-ray range. This result is consistent with expectations for EHSPs, which should have a hard spectrum at high-energies, such as those measured for 1ES 0229+200 and 1ES 1011+496 (Aharonian et al. 2007; Ahnen et al. 2016), the two hardest spectrum sources ever detected in the VHEs. The large spread in spectral points and fit slopes, however, make these considerations on the average trend not representative of all the sample, which appears non-uniform except for the faintness in flux.

4.1 Population considerations

Based on synchrotron peak values reported in the 2WHSP catalogue, the 1BIGB sample holds 52 EHSP candidates, of which 11 objects do not have a firm determination of the peak. We classify the remaining 96 objects of the 1BIGB as (faint) HSP blazars for the purposes of this study.

In order to investigate the properties of EHSP and HSP populations within the catalogue, we have compared the SEDs of the two groups of sources. We find that both the average slope of the EHSP candidates and their spanned fluxes are comparable to those of the HSPs. Therefore, the two populations have no clear signature in the SEDs analyzed which would allow distinguishing them on the basis of their *Fermi*-LAT γ-ray properties alone.

This result suggests that there are EHSPs whose IC peak behaves like standard HSPs, and therefore a shift of the synchrotron peak location to extreme energies does not always reflect in a shift of the second SED peak. Variability most certainly plays an important role on the detectability of these faint sources and a bias towards the presence of high states can contaminate the sample mean, affecting also its spectral properties.

For cases where the second peak is shifted, this could be detected in the VHE regime with the current IACTs or the forthcoming CTA. In any case, the sub-class of EHSPs displaying an IC peak location in the VHE γ-ray range is certainly one of the primary targets of VHE γ-ray observations, and might represent the

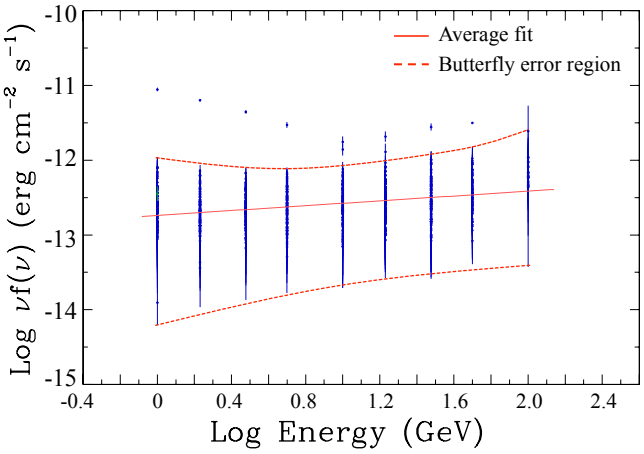

Figure 2. Stacking of the 148 1BIGB SEDs in the 1-100 GeV energy band. Red dashed lines enclose the main flux density interval covered by the measured fluxes and its uncertainties, showing the main region in Log (ν) [GeV] vs. Log (νf_ν) [eg/cm^2/s] covered by the new γ-ray spectrum. Red line is a average power-law fit considering all the 148 SEDs.

Table 3. Most extreme 1BIGB sources (highest synchrotron peak frequency). The index is calculated by fitting a power-law to the SED points in the range 1-100 GeV.

Name	$\Gamma_{1-100\,GeV}$	Log ν^{syn}_{peak}
1BIGB J194356.2+211821	1.68 ± 0.23	18.1
1BIGB J151618.7-152344	2.08 ± 0.07	18.0
1BIGB J225147.5-320611	2.04 ± 0.07	>18.0
1BIGB J020412.9-333339	1.60 ± 0.08	17.9
1BIGB J032056.2+042447	2.65 ± 0.18	17.9
1BIGB J050419.5-095631	2.21 ± 0.08	17.9
1BIGB J055716.7-061706	1.81 ± 0.05	17.9
1BIGB J125341.2-393159	1.72 ± 0.09	17.9
1BIGB J132541.8-022809	1.83 ± 0.15	17.9
1BIGB J160519.0+542058	2.18 ± 0.14	17.9

[3] Please, consult Arsioli & Chang (2017) for a complete list of 1BIGB sources having 2FHL counterparts

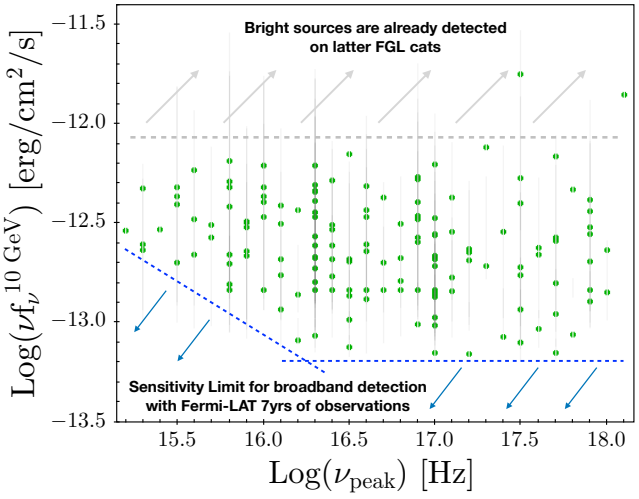

Figure 3. Logarithm of flux density (erg/cm2/s) at 10 GeV vs. logarithm of synchrotron peak frequency (Hz) for the 148 1BIGB sources considered in the study. Dashed lines show the previous (gray) and improved (blue) sensitivity limits.

only class of blazar sources partially undetected by *Fermi*-LAT, but well within the reach of IACTs.

4.2 Sensitivity limit

The 1BIGB sources give us the opportunity to study the sensitivity limit for the γ-ray detection of HSP and EHSP blazars with *Fermi*-LAT. Figure 3 shows the flux density at 10 GeV as a function of the synchrotron peak position taken from the 2WHSP catalogue. Except for two peculiar cases, all sources are contained within a region of flux density at 10 GeV comprised between $10^{-12.1}$ erg/cm^2/s and $10^{-13.2}$ erg/cm^2/s. The sources presented in the 1BIGB catalogue explore a new range of sensitivity, previously not accessible to *Fermi*-LAT catalogs due to the lower exposure time (4 years, in case of the 3FGL).

The cut at the bottom left corner seems to represent the increasing difficulty for detecting sources with the lowest synchrotron Log (ν^{Syn}_{peak}) values. A possible explanation is that for low synchrotron-peak values, the IC peak may move to lower energies, hindering the detections; but also this could be connected to incompleteness of the 2WHSP sample close to the synchrotron peak cut, at $\nu \sim 10^{15}$ Hz. As reported in Chang et al. (2017) the incompleteness might be induced by the multi-frequency selection criteria which was used to build the 2WHSP sample.

4.3 Notable sources

The stacked γ-ray SEDs displayed in Figure 2 present two distinct outliers, namely the sources 1BIGB J224910.6-130002 and 1BIGB J194356.2+211821.

The source 1BIGB J224910.6-130002, also known as RBS 1899, is a blazar of unknown redshift classified as an EHSP due to its synchrotron peak position estimated at $10^{17.5}$ Hz. Interestingly the *Fermi*-LAT spectrum obtained with over 9.3 years of data shows a steep decaying behavior in Log (ν) versus Log (νF_ν) space, with photon spectral index $\Gamma \sim 2.33$ and relatively bright in γ rays, as seen in Figure 4a. However this unusual behavior is probably due to the averaging of the quiescent state with a series of γ-ray flares which happened along 2016 to 2017, as can be seen in the light curve reported in Figure 4b. During these flaring episodes, the flux increased of ~40 times with respect to the quiescent phase. This may also explain why the source was undetected in previous FGL and FHL catalogues. This is an important example of a γ-ray blazar which could represent a major target for the future CTA during periods of extreme activity (as detected during MJD 57662 - 57687, Figure 4a in black). It also illustrates the strong impact of flaring activity in attempting a population study of extreme or faint blazars, since the most extreme γ-ray activity is smoothed over time when integrating over years of *Fermi*-LAT observations.

The second peculiar source, 1BIGB J194356.2+211821 also known as HESS J1943+213, is the most extreme blazar of the 1BIGB catalogue, with Log (ν_p) = 18.1. It was serendipitously discovered by the H.E.S.S. Collaboration (H.E.S.S. Collaboration et al. 2011) at VHE γ rays during a galactic plane survey and later confirmed with VERITAS observations (Shahinyan & VERITAS Collaboration 2015). Due to the source's position on the galactic plane and its multi-wavelength properties, the classification was difficult and three competing hypotheses were proposed: a pulsar wind nebula (PWN), a γ-ray binary, and a blazar, with the latter being favored. Previous studies tried to analyse *Fermi*-LAT data in order to determine the nature of the source: Tanaka et al. (2014b) analysed Pass 7 data on the position of the HESS source, finding a weak detection (TS=22.3) in the 10-300 GeV range, with a rather soft spectral index of $\Gamma \approx 2.4$; analysis of the Pass 7 Reprocessed data (Peter et al. 2014) shows a detection near the position determined by HESS with TS=36.0 in the range 1-300 GeV, and a spectral index of $\Gamma = 1.59$ (in agreement with the value reported here considering the errors). Both these studies favor the blazar interpretation based on multiwavelength data and further observations seem to corroborate this (see e.g. Straal et al. (2016) and Akiyama et al. (2016)), making this the first blazar serendipitously detected by VHE γ-ray ground-based instruments. Interestingly, the optical and UV properties alone would not be enough to classify this source as a blazar, showing the importance of the multi-wavelength approach. The SED in Figure 5 shows that the VHE γ-ray data is complemented nicely by our *Fermi*-LAT points, making the IC peak location clearly above few hundred GeV.

Table 4. Five sources selected for the VHE γ-ray extrapolation study.

1BIGB J Source Name	z	log ν_p	Γ	Cut-off
090802.2−095936	0.053	17.6	1.65 ± 0.13	600 GeV
151041.0+333503	0.114	>17.5	1.92 ± 0.15	300 GeV
225147.5−320611	0.139	>18	2.04 ± 0.07	1 TeV
220155.8−170700	0.169	17.7	0.90 ± 0.15	150 GeV
223301.0+133601	0.214	>17	1.76 ± 0.15	1 TeV

5 POTENTIAL FOR VHE γ-RAY OBSERVATIONS

The individual SEDs of the 1BIGB sources can be exploited to estimate the detectability of these blazars at VHE γ rays. To illustrate this possibility, we have selected five promising objects. The choice of sources was done considering only those objects with known redshift, in order to correctly estimate the absorption of VHE γ-rays due to the interaction with the extragalactic background light, EBL (Stecker et al. 1992). Among those, we considered only blazars with a hard *Fermi*-LAT photon spectral index ($\Gamma < 2.0$). The se-

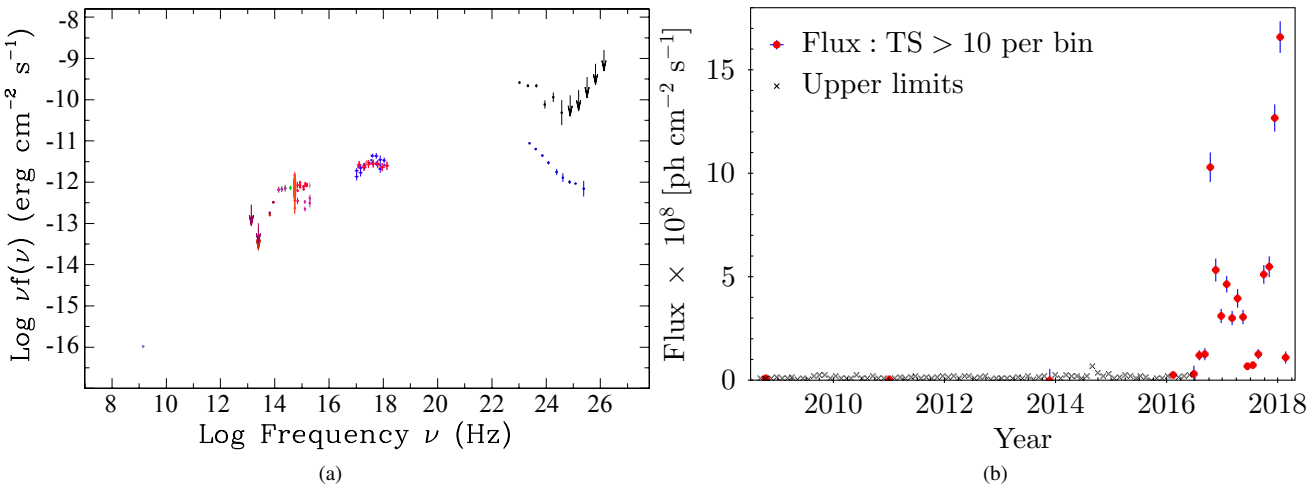

Figure 4. Left plot: SED of 1BIGBJ224910.6-130002, showing the mean γ-ray SED obtained by integrating over 9.3 years in blue, and during the 25 days flare peak (MJD 57662.65-57687.65) in black. Right plot: Light curve of 1BIGBJ224910.6-130002 considering one month time bins, integrating over the broadband of 900 MeV up to 500 GeV. Flux calculated only for $> 3\sigma$ bins (red points), error bars and upper limits (black cross) are calculated using Integral method considering 95% of confidence level.

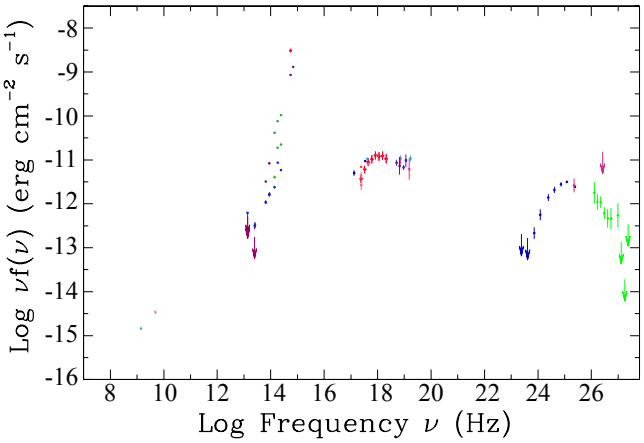

Figure 5. SED of 1BIGB J194356.2+211821. In the γ-ray band we have data points corresponding to our new *Fermi*-LAT detection (in blue), 3FHL (in magenta), and H.E.S.S. (in light green). Notice at 100 GeV the good agreement between 1BIGB (highest energy point) and 3FHL (lowest energy point).

lected sources are listed in Table 4, and ordered by redshift. The table also reports the synchrotron peak location, the *Fermi*-LAT slope obtained from our fit to the 1-100 GeV points, and the cut-off energy of the intrinsic spectrum assumed in our extrapolations.

We would like to note that all selected sources are EHSPs, and mostly this bias result from the synchrotron peak shifting towards high energies, so that the host galaxy thermal component emerge at optical frequencies, allowing a precise redshift measurement.

In Figure 6 we show the γ-ray SEDs of the selected sources up to the highest available energies. We extrapolate the *Fermi*-LAT data points considering a power-law function with exponential cut-off. The cut-off energy for each source was estimated by taking into account all data points and upper limits within the 1-100 GeV energy band. We considered absorption due to interaction with EBL based on $\tau_{E,z}$ values as predicted by Domínguez et al. (2011).

Depending on the location of each source, we have considered detectability with CTA-North and MAGIC, or CTA-South and H.E.S.S. . Each γ-ray SED is represented before (dashed line) and after (dotted-dashed line) EBL absorption. It is evident that the redshift is a very important parameter that can affect sensibly the detectability of blazar candidates. This is particularly true for EHSPs with an IC peak exceeding TeV energies, since in this case, already at relatively small redshifts such as those considered here, the absorption strongly affects the spectrum. The effect is evident in the two sources with the highest assumed cut-off energy, namely 1BIGB J225147.5−320611 and 1BIGB J223301.0+133601 , located at redshift 0.139 and 0.214. Thanks to the relatively high intrinsic emission, despite the EBL absorption severely affecting the observed flux, the extrapolations are still confidently within CTA detectability in both cases.

For 1BIGB J220155.8−170700 the upper limit of $4.19 \cdot 10^{-13}$ erg/cm^2/s at 100 GeV derived from *Fermi*-LAT data severely constrains the location of the IC peak despite the negligible EBL absorption effect, and make this a difficult target even for the expected sensitivity of CTA-North. The last two sources, 1BIGB J151041.0+333503 and 1BIGB J090802.2-095936, present a spectrum compatible with an intrinsic IC peak location at hundreds GeV, and seems on the reach of CTA-North at least in the energy interval close to the SED peak.

All the extrapolated fluxes shown in Figure 6 are well below the sensitivity of current generation of IACTs, indicating that a VHE γ-ray emission from these sources could be detected only in case of extremely bright states.

6 CONCLUSIONS

We have presented for the first time the 1-100 GeV spectrum of a population of γ-ray faint EHSP sources, recently detected with *Fermi*-LAT in the 1BIGB catalogue. The results presented here are an update of the previous 1BIGB work, in the sense that we now include new PASS8 data integrated over 9.3 instead of 7.2 years of observations. This is the largest catalogue of ex-

treme and weak blazars observed in γ rays. All the data presented here is made available in VO tables via the Brazilian Science Data Center (BSDC) service (www.bsdc.cbpf.br), maintained at CBPF, and the BSDC Virtual Observatory (vo.bsdc.icranet.org). It is also accessible via the Open Universe Initiative Portal (www.openuniverse.asi.it) and through the SSDC SED Builder tool (tools.asdc.asi.it).

The 1BIGB sample discussed in this work consists of both HSP and EHSP blazars, whose spectral signatures in the *Fermi*-LAT band were shown to be similar among the two classes, and likely dependent on the source state. No spectral template for the classes was derivable, nevertheless we call attention to fact that the sample is limited in size and inhomogeneous.

The average observed spectral index in the 1-100 GeV band ranges between 1.3 and 2.8 indicating a predominantly hard spectrum. The average flux of the extreme HSP sample is relatively low, being composed of weak sources at the limit of the *Fermi*-LAT sensitivity. For these reasons we argue that EHSPs may escape *Fermi*-LAT detection (or be detected with low significance only), but still be prime candidates for observations with Cherenkov telescopes, due to the expected high VHE γ-ray emission. As we showed, it is expected for at least part of the objects, that the IC peak will fall well within the VHE band, above 100 GeV. Methods of selecting EHSPs not based exclusively on *Fermi*-LAT detections or extrapolations are therefore extremely interesting for completing the extragalactic population to be targeted by CTA.

In fact, we performed a detailed study of the potential for VHE γ-ray observations of the strongest 1BIGB sources with known redshift, indicating that they are well within the reach of future CTA capabilities. These analyses show that future VHE observations are in a good position to probe this poorly known, extreme class of HSP sources, expanding our understanding of the blazar phenomenon and bringing new elements to the framework of the blazar sequence scenario.

ACKNOWLEDGEMENTS

During this work, BA was supported by São Paulo Research Foundation (FAPESP) with grant n. 2017/00517-4. UBdA acknowledges support from a FAPERJ Young Scientist Fellowship n. E10/2016-226465 and a CNPq Level 2 Fellowship n. 310827/2016-7. BF is supported by FAPERJ grants n. 202.687/2016 and 202.688/2016. We would like to thanks Prof. Marcelo M. Guzzo and Prof. Orlando L. G. Peres for the full support endorsing the author's partnership with FAPESP, and granting access to the Feynman Cluster from CCJDR Data Center at IFGW Unicamp, Campinas-Brazil. We also thank IcraNet, Prof. Remo Ruffini and Prof. Carlo Bianco for the cooperation granting access to Joshua Computer Cluster (Rome-Italy). The availability of computational resources was key to the development of our work. We make use of archival data and bibliographic information obtained from the NASA-IPAC Extragalactic Database (NED), data, and software facilities from the Space Science Data Center (SSDC) from the Italian Space Agency. The VO publication of our data (vo.bsdc.icranet.org) is made by the Brazilian Science Data Center (BSDC) service maintained at CBPF, Rio de Janeiro, and accessible through the United Nations Open Universe Initiative at http://www.openuniverse.asi.it. We thank Mr. Carlos Brandt for his support on this task. This research has made use of the CTA instrument response functions provided by the CTA Consortium and Observatory, see http://www.cta-observatory.org/science/cta-performance/ (version prod3b-v1) for more details.

REFERENCES

Abdo A. A., et al., 2010a, ApJS, 188, 405
Abdo A. A., et al., 2010b, The Astrophysical Journal, 716, 30
Acero F., et al., 2015, ApJS, 218, 23
Ackermann M., et al., 2015, ApJ, 799, 86
Ackermann M., et al., 2016, ApJS, 222, 5
Aharonian F., et al., 2006, A&A, 457, 899
Aharonian F., et al., 2007, A&A, 475, L9
Ahnen M. L., et al., 2016, A&A, 590, A24
Ajello M., et al., 2017, ApJS, 232, 18
Akiyama K., Stawarz Ł., Tanaka Y. T., Nagai H., Giroletti M., Honma M., 2016, ApJ, 823, L26
Aleksić J., et al., 2016, Astroparticle Physics, 72, 76
Arsioli B., Chang Y.-L., 2017, A&A, 598, A134
Arsioli B., Polenta G., 2018, preprint, (arXiv:1804.03703)
Arsioli B., Fraga B., Giommi P., Padovani P., Marrese P. M., 2015, A&A, 579, A34
Atwood W., et al., 2013, preprint, (arXiv:1303.3514)
Bonnoli G., Tavecchio F., Ghisellini G., Sbarrato T., 2015, MNRAS, 451, 611
Böttcher M., Reimer A., Sweeney K., Prakash A., 2013, ApJ, 768, 54
CTA Consortium T., et al., 2017, preprint, (arXiv:1709.07997)
Cerruti M., Zech A., Emery G., Guarin D., 2017, in 6th International Symposium on High Energy Gamma-Ray Astronomy. p. 050027 (arXiv:1610.00255), doi:10.1063/1.4968973
Chang Y.-L., Arsioli B., Giommi P., Padovani P., 2017, A&A, 598, A17
Costamante L., Ghisellini G., 2002, A&A, 384, 56
Costamante L., et al., 2001, A&A, 371, 512
Costamante L., Bonnoli G., Tavecchio F., Ghisellini G., Tagliaferri G., Khangulyan D., 2017, preprint, (arXiv:1711.06282)
Danforth C. W., Keeney B. A., Stocke J. T., Shull J. M., Yao Y., 2010, ApJ, 720, 976
Domínguez A., et al., 2011, MNRAS, 410, 2556
Fossati G., Maraschi L., Celotti A., Comastri A., Ghisellini G., 1998, MNRAS, 299, 433
Furniss A., et al., 2013, ApJ, 768, L31
Ghisellini G., 1999, Astroparticle Physics, 11, 11
Ghisellini G., Righi C., Costamante L., Tavecchio F., 2017, MNRAS, 469, 255
H.E.S.S. Collaboration et al., 2011, A&A, 529, A49
Inoue Y., Ioka K., 2012, Phys. Rev. D, 86, 023003
Kaufmann S., Wagner S. J., Tibolla O., Hauser M., 2011, A&A, 534, A130
Masetti N., et al., 2013, A&A, 559, A58
Massaro E., Maselli A., Leto C., Marchegiani P., Perri M., Giommi P., Piranomonte S., 2015, Ap&SS, 357
Mattox J. R., et al., 1996, ApJ, 461, 396
Nolan P. L., et al., 2012, ApJS, 199, 31
Padovani P., Giommi P., 1995, ApJ, 444, 567
Padovani P., Resconi E., Giommi P., Arsioli B., Chang Y. L., 2016, MNRAS, 457, 3582
Padovani P., et al., 2017, A&ARv, 25, 2
Padovani P., Giommi P., Resconi E., Glauch T., Arsioli B., Sahakyan N., 2018, NMRAS, in preparation
Peter D., Domainko W., Sanchez D. A., van der Wel A., Gässler W., 2014, A&A, 571, A41
Pita S., et al., 2014, A&A, 565, A12
Resconi E., Coenders S., Padovani P., Giommi P., Caccianiga L., 2017, MNRAS, 468, 597
Sbarufatti B., Treves A., Falomo R., Heidt J., Kotilainen J., Scarpa R., 2005, AJ, 129, 559
Shahinyan K., VERITAS Collaboration 2015, in 34th International Cosmic Ray Conference (ICRC2015). p. 878

Shaw M. S., Filippenko A. V., Romani R. W., Cenko S. B., Li W., 2013a, AJ, 146, 127
Shaw M. S., et al., 2013b, ApJ, 764, 135
Sol H., et al., 2013, Astroparticle Physics, 43, 215
Stecker F. W., de Jager O. C., Salamon M. H., 1992, ApJ, 390, L49
Straal S. M., Gabányi K. É., van Leeuwen J., Clarke T. E., Dubner G., Frey S., Giacani E., Paragi Z., 2016, ApJ, 822, 117
Tanaka Y. T., et al., 2014a, ApJ, 787, 155
Tanaka Y. T., et al., 2014b, ApJ, 787, 155
Tavecchio F., Ghisellini G., Bonnoli G., Foschini L., 2011, MNRAS, 414, 3566
Urry C. M., Padovani P., 1995, PASP, 107, 803

APPENDIX A: THE 1BIGB COMPLETE TABLE WITH BROADBAND FITTING INFORMATION

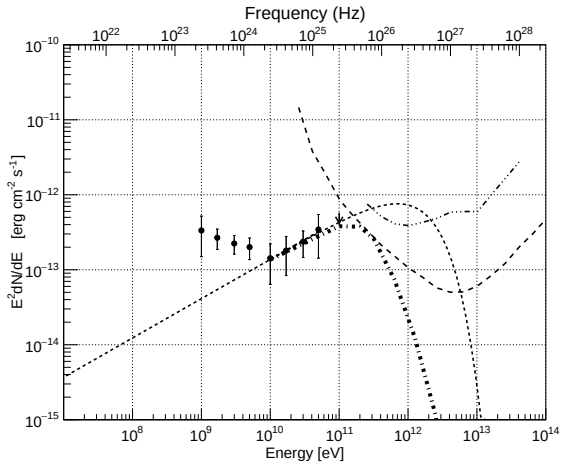

(a) 1BIGB J225147.5−320611 extrapolated with power-law and cut-off at 700 GeV.

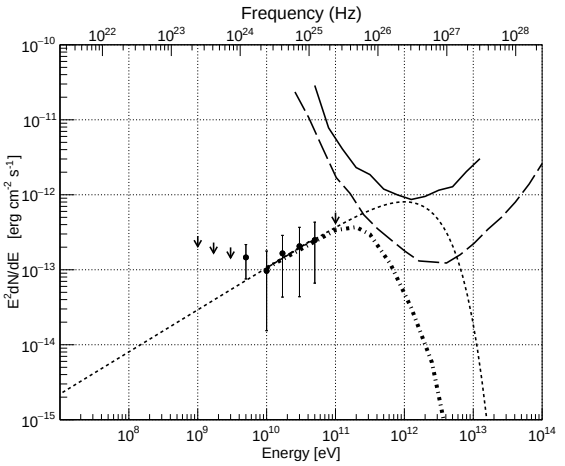

(b) 1BIGB J223301.0+133601 extrapolated with power-law and cut-off at 1 TeV.

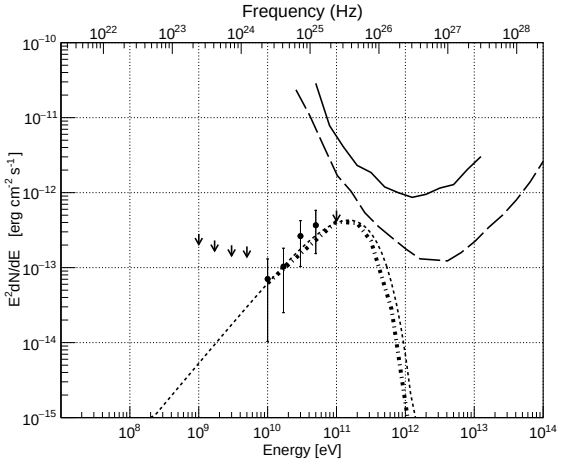

(c) 1BIGB J220155.8−170700 extrapolated with power-law and cut-off at 150 GeV.

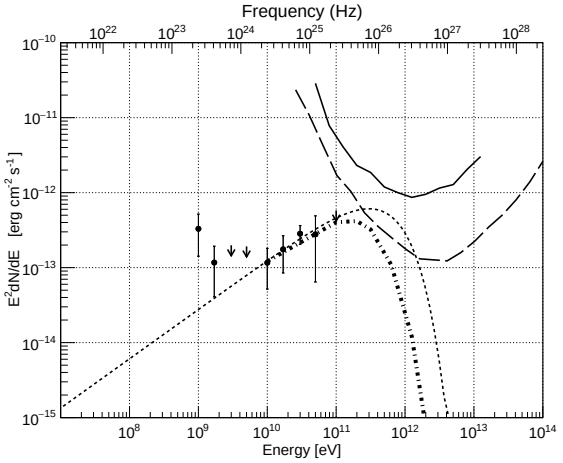

(d) 1BIGB J151041.0+333503 extrapolated with power-law and cut-off at 300 GeV.

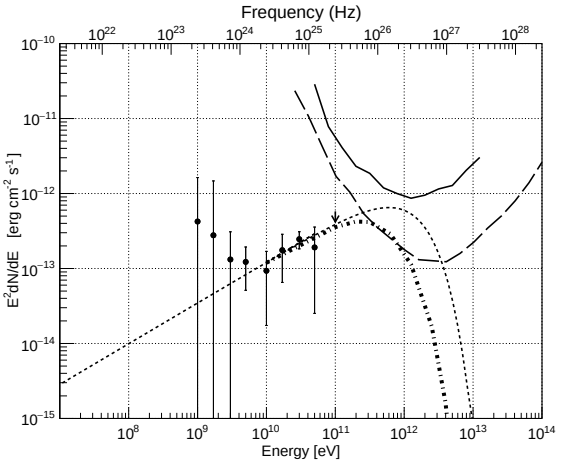

(e) 1BIGB J090802.2−095936 extrapolated with power-law and cut-off at 600 GeV.

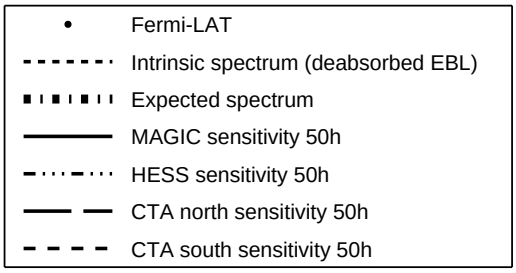

(f) Legend.

Figure 6. Extrapolation of the γ-ray spectrum of five selected sources of the 1BIGB catalogue. The intrinsic spectrum assumed is a power-law with an exponential cut-off (dashed line). The resulting spectra once corrected for EBL absorption are displayed with dashed-dotted lines. CTA, MAGIC (Aleksić et al. 2016), and H.E.S.S. (Aharonian et al. 2006) sensitivities for 50 h of observations are also reported in the plots.

Table A1. Table showing the 148 1BIGB γ-ray signatures. The first three columns show respectively the 1BIGB source names, right ascension R.A. and declination Dec. in degrees (J2000). The fourth column shows the reported redshifts from literature (Shaw et al. 2013b; Pita et al. 2014; Furniss et al. 2013; Danforth et al. 2010; Shaw et al. 2013a; Masetti et al. 2013; Sbarufatti et al. 2005; Massaro et al. 2015), flag ? is used for values reported as uncertain; lower limit are marked with ">" (all lower-limits shown here were derived in Arsioli et al. 2015; Chang et al. 2017), and sources with currently absent redshift were given 0. value. The γ-ray model parameters from Fermi Science Tools assume a power law to describe the spectrum within the studied energy range 0.3-500 GeV. The parameter N_0 (see eq. 1) is given in units of [ph/cm^2/s/MeV], and Γ is the spectral photon index, which are direct outputs from the likelihood analysis over 7.2 years of Fermi-LAT data in the 0.3-500 GeV band; those results consider the pivot energy fixed as $E_0 = 1$ GeV. The column Flux gives the photon counts in units of ph/cm^2/s calculated by integrating eq. 1 along the energy range 1-100 GeV, column E-FLux corresponds to the energy flux in units of MeV/cm^2/s. For the columns Flux and E-flux, upper and lower case values represent positive and negative errors, respectively.

1BIGB Source name	R.A.(deg)	Dec.(deg)	z	Γ	N_0 (10^{-15})	TS	Flux$^{\times 10^{-10}}_{1-100GeV}$	E-Flux$^{\times 10^{-13}}_{1-100GeV}$
1BIGBJ000949.6-431650	2.45708	-43.28056	>0.56	2.19±0.13	2.29±0.40	86.2	$1.92^{0.63}_{-0.50}$	$7.0^{2.3}_{-1.5}$
1BIGBJ001328.8+094929	3.37	9.825	0.	2.07±0.19	1.56±0.57	24.6	$1.44^{0.95}_{-0.67}$	$6.0^{3.5}_{-1.9}$
1BIGBJ001527.8+353638	3.86625	35.61083	>0.57	1.90±0.23	0.94±0.48	35.3	$1.02^{0.99}_{-0.62}$	$5.4^{4.7}_{-2.2}$
1BIGBJ002928.6+205332	7.36917	20.8925	0.	1.66±0.19	0.59±0.31	29.5	$0.85^{0.87}_{-0.53}$	$6.5^{5.3}_{-2.7}$
1BIGBJ004146.9-470136	10.44583	-47.02667	0.	1.79±0.27	0.33±0.21	10.8	$0.40^{0.55}_{-0.30}$	$2.5^{3.0}_{-1.2}$
1BIGBJ005816.6+172312	14.56958	17.38694	0.	1.79±0.24	0.73±0.44	24.0	$0.89^{1.07}_{-0.62}$	$5.6^{5.7}_{-2.5}$
1BIGBJ010250.8-200158	15.71208	-20.03278	>0.38	1.49±0.23	0.25±0.17	20.4	$0.45^{0.68}_{-0.35}$	$4.6^{5.2}_{-2.2}$
1BIGBJ011501.6-340027	18.75708	-34.0075	0.48	1.65±0.16	0.82±0.36	70.8	$1.19^{0.98}_{-0.64}$	$9.2^{6.1}_{-3.4}$
1BIGBJ012657.1+330730	21.73833	33.125	0.	2.19±0.29	1.38±0.57	22.2	$1.15^{0.99}_{-0.61}$	$4.2^{3.9}_{-1.6}$
1BIGBJ014040.8-075849	25.17	-7.98028	>0.49	1.77±0.14	1.12±0.37	45.0	$1.41^{0.85}_{-0.61}$	$9.1^{4.7}_{-2.9}$
1BIGBJ020106.1+003400	30.27542	0.56667	0.298	1.70±0.24	0.47±0.30	19.9	$0.65^{0.84}_{-0.47}$	$4.7^{5.0}_{-2.2}$
1BIGBJ020412.9-333339	31.05375	-33.56111	0.617	1.85±0.19	0.87±0.35	31.7	$1.00^{0.78}_{-0.51}$	$5.7^{4.1}_{-2.1}$
1BIGBJ021205.6-255757	33.02375	-25.96611	0.	1.99±0.14	1.67±0.41	58.9	$1.67^{0.74}_{-0.56}$	$7.8^{3.3}_{-2.1}$
1BIGBJ021216.8-022155	33.07	-2.36528	0.	1.92±0.19	1.16±0.44	31.8	$1.23^{0.89}_{-0.60}$	$6.3^{4.3}_{-2.3}$
1BIGBJ021631.9+231449	34.13333	23.24722	0.288	1.88±0.10	2.49±0.52	116.4	$2.76^{0.98}_{-0.79}$	$15.0^{4.7}_{-3.3}$
1BIGBJ022048.4-084250	35.20167	-8.71389	>0.43	1.88±0.20	1.00±0.43	34.1	$1.11^{0.90}_{-0.59}$	$6.0^{4.3}_{-2.2}$
1BIGBJ023340.9+065611	38.42042	6.93639	0.	2.03±0.14	3.23±0.90	98.0	$3.08^{1.45}_{-1.12}$	$13.6^{5.4}_{-3.5}$
1BIGBJ023430.5+804336	38.6275	80.72694	0.	1.55±0.14	0.37±0.16	32.4	$0.63^{0.49}_{-0.34}$	$5.8^{3.2}_{-1.9}$
1BIGBJ030103.7+344100	45.26542	34.68361	0.24	2.33±0.16	3.26±0.63	56.3	$2.43^{0.87}_{-0.68}$	$7.6^{2.7}_{-1.7}$
1BIGBJ030330.1+055429	45.87542	5.90833	0.196	1.50±0.23	0.33±0.26	24.5	$0.60^{0.99}_{-0.51}$	$6.0^{7.0}_{-3.0}$
1BIGBJ030433.9-005403	46.14125	-0.90111	0.511	1.69±0.16	0.79±0.35	38.1	$1.09^{0.87}_{-0.59}$	$7.9^{5.0}_{-2.8}$
1BIGBJ030544.1+403509	46.43375	40.58611	0.	1.88±0.25	0.77±0.46	19.0	$0.85^{0.98}_{-0.58}$	$4.6^{4.5}_{-2.0}$
1BIGBJ031103.1-440227	47.76333	-44.04111	0.	1.96±0.35	0.72±0.43	16.4	$0.73^{1.03}_{-0.52}$	$3.5^{5.5}_{-1.8}$
1BIGBJ031423.8+061955	48.59958	6.33222	0.62?	1.78±0.11	2.25±0.58	92.4	$2.78^{1.22}_{-0.95}$	$17.6^{6.4}_{-4.4}$
1BIGBJ032009.1-704533	50.03833	-70.75917	0.	1.77±0.18	0.63±0.26	32.1	$0.79^{0.63}_{-0.41}$	$5.1^{3.5}_{-1.9}$
1BIGBJ032037.9+112451	50.15833	11.41444	0.	2.36±0.24	3.12±0.99	24.8	$2.27^{1.35}_{-0.95}$	$6.9^{3.9}_{-2.1}$
1BIGBJ032056.2+042447	50.23458	4.41333	0.	2.70±0.22	3.03±0.61	30.1	$1.78^{0.69}_{-0.52}$	$4.1^{1.5}_{-0.9}$
1BIGBJ032647.2-340446	51.69708	-34.07972	0.	2.04±0.12	1.96±0.38	76.7	$1.86^{0.64}_{-0.51}$	$8.1^{2.7}_{-1.8}$
1BIGBJ032852.6-571605	52.21917	-57.26806	0.	1.55±0.18	0.36±0.19	36.3	$0.61^{0.65}_{-0.39}$	$5.6^{4.6}_{-2.4}$
1BIGBJ033623.7-034738	54.09875	-3.79389	0.162	1.44±0.19	0.36±0.23	41.6	$0.71^{0.93}_{-0.52}$	$7.8^{7.1}_{-3.5}$
1BIGBJ033831.9-570447	54.63333	-57.08	0.	1.89±0.27	0.43±0.25	10.6	$0.48^{0.56}_{-0.32}$	$2.5^{2.8}_{-1.1}$
1BIGBJ035856.1-305447	59.73375	-30.91306	0.65?	1.92±0.14	1.43±0.40	59.6	$1.53^{0.76}_{-0.57}$	$7.9^{3.6}_{-2.2}$
1BIGBJ041112.2-394143	62.80125	-39.69528	>0.7	1.74±0.29	0.23±0.19	6.7	$0.31^{0.53}_{-0.26}$	$2.1^{3.0}_{-1.1}$
1BIGBJ041238.3-392629	63.16	-39.44139	0.	1.91±0.30	0.34±0.25	6.7	$0.37^{0.54}_{-0.29}$	$1.9^{2.5}_{-9.5}$
1BIGBJ042900.1-323641	67.25042	-32.61139	>0.51	2.04±0.17	1.20±0.36	27.9	$1.13^{0.63}_{-0.45}$	$4.9^{2.6}_{-1.5}$
1BIGBJ043517.7-262121	68.82375	-26.35611	0.	2.60±0.28	1.64±0.43	20.2	$1.02^{0.54}_{-0.38}$	$2.5^{1.4}_{-0.7}$
1BIGBJ044127.4+150454	70.36417	15.08194	0.109	2.10±0.18	3.03±1.18	43.0	$2.74^{1.81}_{-1.30}$	$11.1^{6.0}_{-3.4}$
1BIGBJ044240.6+614039	70.66917	61.6775	0.	2.01±0.09	4.00±0.71	145.0	$3.92^{1.12}_{-0.95}$	$17.9^{4.3}_{-3.2}$
1BIGBJ044328.3-415156	70.86833	-41.86556	>0.39	1.96±0.15	1.58±0.44	66.8	$1.63^{0.83}_{-0.61}$	$8.0^{3.8}_{-2.3}$
1BIGBJ050335.3-111506	75.8975	-11.25167	>0.57	1.85±0.11	2.30±0.53	102.6	$2.63^{1.03}_{-0.82}$	$15.0^{5.1}_{-3.5}$
1BIGBJ050419.5-095631	76.08125	-9.94222	>0.46	2.14±0.23	1.29±0.54	16.6	$1.12^{0.86}_{-0.58}$	$4.3^{3.0}_{-1.5}$
1BIGBJ050601.6-382054	76.50667	-38.34861	0.182	1.95±0.11	2.06±0.40	96.5	$2.13^{0.73}_{-0.59}$	$10.5^{3.4}_{-2.4}$
1BIGBJ050727.1-334635	76.86333	-33.77639	0.	1.79±0.11	1.84±0.43	125.0	$2.25^{0.93}_{-0.72}$	$14.1^{5.0}_{-3.5}$
1BIGBJ053626.8-254748	84.11167	-25.79667	0.	2.06±0.16	1.70±0.44	47.9	$1.58^{0.76}_{-0.56}$	$6.7^{3.1}_{-1.9}$
1BIGBJ053645.2-255841	84.18875	-25.97806	0.	1.92±0.18	1.20±0.44	33.8	$1.28^{0.88}_{-0.60}$	$6.6^{4.2}_{-2.3}$
1BIGBJ055716.7-061706	89.32	-6.285	0.	1.95±0.15	2.51±0.86	52.2	$2.59^{1.52}_{-1.12}$	$12.7^{6.3}_{-3.8}$
1BIGBJ060714.2-251859	91.80958	-25.31639	0.275	1.94±0.14	1.54±0.40	51.9	$1.61^{0.75}_{-0.57}$	$8.1^{3.4}_{-2.2}$
1BIGBJ062149.6-341148	95.45667	-34.19694	0.529	2.53±0.12	4.77±0.59	93.3	$3.09^{0.68}_{-0.58}$	$8.1^{1.6}_{-1.2}$
1BIGBJ062626.2-171045	96.60917	-17.17944	>0.7	2.00±0.18	1.80±0.66	34.6	$1.78^{1.17}_{-0.82}$	$8.2^{4.9}_{-2.7}$
1BIGBJ063014.9-201236	97.5625	-20.21	0.	1.56±0.33	0.37±0.47	16.2	$0.62^{1.79}_{-0.72}$	$5.6^{11.0}_{-3.3}$
1BIGBJ065932.8-674350	104.88708	-67.73056	0.	1.63±0.17	0.55±0.29	39.4	$0.82^{0.78}_{-0.50}$	$6.5^{4.6}_{-2.5}$

Table A2. Continued.

1BIGB Source name	R.A.(deg)	Dec.(deg)	z	Γ	N_0 (10^{-15})	TS	Flux$^{\times 10^{-10}}_{1-100GeV}$	E-Flux$^{\times 10^{-13}}_{1-100GeV}$
1BIGBJ071745.0-552021	109.4375	-55.33944	0.	2.12±0.14	2.32±0.53	60.9	$2.05^{0.83}_{-0.65}$	$8.1^{3.0}_{-2.0}$
1BIGBJ073152.6+280432	112.96958	28.07583	0.248	1.90±0.18	1.06±0.39	29.9	$1.15^{0.79}_{-0.54}$	$6.1^{3.8}_{-2.1}$
1BIGBJ073329.5+351542	113.37292	35.26167	0.177	2.56±0.23	1.71±0.42	21.0	$1.09^{0.51}_{-0.37}$	$2.8^{1.2}_{-0.7}$
1BIGBJ075936.1+132116	119.90042	13.35472	0.	1.75±0.09	2.12±0.44	152.6	$2.71^{0.98}_{-0.79}$	$17.9^{5.5}_{-4.0}$
1BIGBJ080015.4+561107	120.06458	56.18528	0.	1.92±0.12	1.54±0.34	78.9	$1.65^{0.65}_{-0.51}$	$8.5^{3.1}_{-2.1}$
1BIGBJ082904.7+175415	127.27	17.90417	0.089	2.25±0.10	4.47±0.55	136.8	$3.55^{0.79}_{-0.67}$	$12.1^{2.7}_{-2.0}$
1BIGBJ083724.5+145819	129.3525	14.97222	0.278	1.75±0.15	1.07±0.37	50.6	$1.37^{0.87}_{-0.61}$	$9.1^{4.9}_{-2.9}$
1BIGBJ085749.8+013530	134.4575	1.59167	0.281	2.57±0.23	1.81±0.48	18.6	$1.15^{0.56}_{-0.42}$	$2.9^{1.3}_{-0.7}$
1BIGBJ090802.2-095936	137.00917	-9.99361	0.053	1.79±0.26	0.68±0.49	22.5	$0.83^{1.17}_{-0.65}$	$5.2^{5.8}_{-2.4}$
1BIGBJ090953.2+310602	137.47167	31.10083	0.272	1.81±0.21	0.62±0.32	22.3	$0.75^{0.73}_{-0.45}$	$4.5^{3.7}_{-1.8}$
1BIGBJ091322.3+813305	138.34292	81.55139	0.639?	1.40±0.15	0.20±0.10	41.5	$0.42^{0.42}_{-0.26}$	$4.9^{3.4}_{-1.9}$
1BIGBJ091651.8+523827	139.21625	52.64111	0.19	1.97±0.17	1.17±0.35	60.6	$1.18^{0.67}_{-0.48}$	$5.7^{3.1}_{-1.8}$
1BIGBJ093239.2+104234	143.16375	10.70972	0.361	2.00±0.14	1.95±0.49	58.5	$1.92^{0.87}_{-0.66}$	$8.9^{3.7}_{-2.4}$
1BIGBJ093430.1-172120	143.62542	-17.35583	0.	1.75±0.22	0.79±0.50	20.9	$1.02^{1.22}_{-0.72}$	$6.7^{6.4}_{-2.9}$
1BIGBJ095224.1+750212	148.10042	75.03694	0.181	1.43±0.15	0.29±0.14	62.4	$0.57^{0.54}_{-0.34}$	$6.3^{4.2}_{-2.4}$
1BIGBJ095507.9+355100	148.78292	35.85	0.834	2.00±0.25	0.82±0.38	24.1	$0.80^{0.74}_{-0.46}$	$3.7^{3.3}_{-1.5}$
1BIGBJ095628.2-095719	149.1175	-9.95528	0.	1.80±0.26	0.60±0.40	16.1	$0.73^{0.98}_{-0.54}$	$4.5^{5.2}_{-2.1}$
1BIGBJ095849.8+703959	149.7075	70.66639	0.	1.98±0.23	0.99±0.43	37.1	$0.99^{0.84}_{-0.54}$	$4.7^{3.7}_{-1.8}$
1BIGBJ102100.3+162554	155.25125	16.43167	0.556	2.16±0.23	1.48±0.52	27.9	$1.27^{0.86}_{-0.58}$	$4.8^{3.2}_{-1.6}$
1BIGBJ104303.7+005420	160.76583	0.90556	0.	1.75±0.14	1.30±0.43	56.5	$1.67^{1.00}_{-0.72}$	$11.0^{5.5}_{-3.4}$
1BIGBJ104857.6+500945	162.24	50.1625	0.402	2.37±0.15	2.01±0.35	53.1	$1.46^{0.47}_{-0.38}$	$4.4^{1.4}_{-0.9}$
1BIGBJ105534.3-012616	163.89292	-1.43778	0.	1.66±0.11	1.53±0.43	99.0	$2.20^{1.08}_{-0.82}$	$16.9^{6.6}_{-4.5}$
1BIGBJ111717.5+000633	169.32292	0.10917	0.451	1.92±0.15	1.87±0.53	57.4	$2.00^{1.04}_{-0.76}$	$10.3^{4.9}_{-3.0}$
1BIGBJ112317.9-323217	170.825	-32.53833	0.	2.06±0.22	1.25±0.48	22.8	$1.16^{0.85}_{-0.57}$	$4.9^{3.5}_{-1.7}$
1BIGBJ112611.8-203723	171.54958	-20.62333	0.	2.12±0.27	1.15±0.59	11.6	$1.02^{0.99}_{-0.62}$	$4.0^{3.5}_{-1.6}$
1BIGBJ113046.0-313807	172.69208	-31.63528	0.151	1.29±0.20	0.13±0.10	24.8	$0.33^{0.56}_{-0.28}$	$4.7^{5.0}_{-2.3}$
1BIGBJ113105.2-094405	172.77167	-9.735	0.	1.66±0.14	0.99±0.35	64.1	$1.43^{0.92}_{-0.65}$	$10.9^{5.7}_{-3.5}$
1BIGBJ113444.6-172900	173.68625	-17.48361	0.571	1.68±0.17	0.79±0.35	36.9	$1.10^{0.91}_{-0.60}$	$8.2^{5.4}_{-3.0}$
1BIGBJ113755.6-171041	174.48167	-17.17833	0.6	1.71±0.10	1.90±0.43	126.9	$2.55^{1.00}_{-0.79}$	$18.0^{6.0}_{-4.2}$
1BIGBJ121158.6+224233	182.99417	22.70917	0.45	1.83±0.17	0.89±0.34	30.2	$1.04^{0.74}_{-0.50}$	$6.0^{3.8}_{-2.1}$
1BIGBJ121510.9+073203	183.79542	7.53444	0.137	1.64±0.11	1.26±0.37	105.5	$1.87^{0.97}_{-0.72}$	$14.9^{6.2}_{-4.1}$
1BIGBJ121603.1-024304	184.01333	-2.71778	0.169	2.22±0.16	2.81±0.67	56.3	$2.28^{0.97}_{-0.74}$	$8.0^{3.2}_{-2.0}$
1BIGBJ124141.4+344029	190.4225	34.675	>0.7	1.88±0.15	1.19±0.37	46.8	$1.33^{0.76}_{-0.55}$	$7.3^{3.8}_{-2.3}$
1BIGBJ125015.4+315559	192.56458	31.93306	0.	1.82±0.31	0.55±0.39	16.8	$0.65^{1.02}_{-0.51}$	$3.9^{5.7}_{-2.0}$
1BIGBJ125341.2-393159	193.42167	-39.53306	0.179	1.89±0.17	1.29±0.51	39.8	$1.42^{1.00}_{-0.69}$	$7.6^{4.6}_{-2.6}$
1BIGBJ125847.9-044744	194.7	-4.79583	0.586?	1.93±0.11	2.50±0.62	61.2	$2.64^{1.10}_{-0.87}$	$13.5^{4.7}_{-3.2}$
1BIGBJ130145.6+405623	195.44	40.94	0.652	2.18±0.15	2.04±0.40	71.5	$1.71^{0.63}_{-0.49}$	$6.3^{2.3}_{-1.5}$
1BIGBJ130713.3-034430	196.80542	-3.74194	0.	2.05±0.26	1.14±0.57	19.0	$1.08^{1.03}_{-0.64}$	$4.7^{4.2}_{-1.9}$
1BIGBJ132541.8-022809	201.42417	-2.46944	0.8?	1.93±0.18	1.13±0.42	27.3	$1.19^{0.80}_{-0.56}$	$6.0^{3.6}_{-2.0}$
1BIGBJ132617.7+122957	201.57375	12.49944	0.204	2.08±0.20	1.57±0.50	32.2	$1.44^{0.87}_{-0.61}$	$6.0^{3.6}_{-1.9}$
1BIGBJ132833.4+114520	202.13958	11.75556	0.811	1.92±0.17	1.31±0.46	37.5	$1.40^{0.90}_{-0.63}$	$7.1^{4.1}_{-2.3}$
1BIGBJ133612.1+231958	204.05042	23.33278	0.267	1.97±0.15	1.66±0.42	62.5	$1.68^{0.79}_{-0.59}$	$8.0^{3.6}_{-2.3}$
1BIGBJ135328.0+560056	208.36667	56.01556	0.404	2.25±0.15	2.13±0.42	71.0	$1.69^{0.61}_{-0.48}$	$5.7^{2.0}_{-1.3}$
1BIGBJ140629.9-393508	211.625	-39.58583	0.37	1.54±0.16	0.56±0.27	42.7	$0.96^{0.87}_{-0.56}$	$9.0^{5.9}_{-3.3}$
1BIGBJ143342.7-730437	218.42792	-73.07722	0.	1.33±0.20	0.15±0.11	24.6	$0.36^{0.55}_{-0.29}$	$4.7^{4.6}_{-2.2}$
1BIGBJ143825.4+120418	219.60625	12.07167	0.	2.11±0.21	1.35±0.49	25.2	$1.20^{0.82}_{-0.56}$	$4.8^{3.1}_{-1.6}$
1BIGBJ144236.4-462300	220.65167	-46.38361	0.103	1.92±0.10	3.14±0.64	107.7	$3.33^{1.14}_{-0.93}$	$17.1^{5.0}_{-3.6}$
1BIGBJ145543.6-760051	223.93167	-76.01444	0.	1.61±0.12	0.63±0.22	43.7	$0.96^{0.59}_{-0.43}$	$7.9^{3.6}_{-2.3}$
1BIGBJ145603.5+504825	224.015	50.80722	>0.49	2.09±0.24	1.23±0.55	27.2	$1.11^{0.92}_{-0.60}$	$4.5^{3.4}_{-1.6}$
1BIGBJ150637.0-054004	226.65458	-5.66778	0.518	1.72±0.17	0.94±0.41	35.2	$1.25^{1.00}_{-0.67}$	$8.7^{5.5}_{-3.1}$
1BIGBJ151041.0+333503	227.67125	33.58444	0.114	1.59±0.30	0.27±0.24	15.2	$0.43^{0.91}_{-0.40}$	$3.7^{6.4}_{-2.1}$
1BIGBJ151136.8-165326	227.90375	-16.89056	>0.56	2.15±0.35	1.22±0.74	13.1	$1.06^{1.36}_{-0.74}$	$4.0^{5.3}_{-1.8}$
1BIGBJ151618.7-152344	229.07792	-15.39556	>0.54	1.98±0.18	1.50±0.58	27.2	$1.51^{1.02}_{-0.72}$	$7.1^{4.1}_{-2.3}$
1BIGBJ151826.5+075222	229.61083	7.87278	0.41	1.74±0.20	0.66±0.33	24.6	$0.85^{0.81}_{-0.51}$	$5.7^{4.5}_{-2.3}$
1BIGBJ151845.7+061355	229.69042	6.23222	0.102	1.96±0.21	1.36±0.56	31.8	$1.39^{1.09}_{-0.72}$	$6.8^{5.0}_{-2.5}$
1BIGBJ152646.6-153025	231.69417	-15.50722	>0.43	2.04±0.13	2.61±0.64	58.4	$2.47^{1.06}_{-0.82}$	$10.8^{4.1}_{-2.7}$
1BIGBJ152913.5+381216	232.30625	38.20472	>0.59	2.04±0.19	1.22±0.39	34.6	$1.16^{0.69}_{-0.49}$	$5.1^{2.9}_{-1.6}$
1BIGBJ154202.9-291509	235.5125	-29.2525	0.	1.78±0.08	2.62±0.50	143.2	$3.27^{1.04}_{-0.86}$	$20.8^{5.4}_{-4.1}$
1BIGBJ154625.0-285723	236.60417	-28.95639	>0.6	1.73±0.18	0.67±0.36	18.7	$0.88^{0.84}_{-0.54}$	$6.0^{4.3}_{-2.3}$
1BIGBJ155053.2-082245	237.72167	-8.37944	0.	1.87±0.14	1.96±0.63	64.9	$2.20^{1.24}_{-0.91}$	$12.2^{5.8}_{-3.6}$

Table A3. Continued.

1BIGB Source name	R.A.(deg)	Dec.(deg)	z	Γ	N_0 (10^{-15})	TS	Flux$^{\times 10^{-10}}_{1-100GeV}$	E-Flux$^{\times 10^{-13}}_{1-100GeV}$
1BIGBJ155432.5-121324	238.63542	-12.22361	0.	1.69±0.13	1.04±0.39	34.3	$1.45^{0.94}_{-0.68}$	$10.6^{5.3}_{-3.3}$
1BIGBJ160218.0+305108	240.575	30.8525	>0.47	2.44±0.27	1.83±0.47	33.8	$1.27^{0.70}_{-0.48}$	$3.6^{2.3}_{-1.1}$
1BIGBJ160519.0+542058	241.32917	54.34972	0.212	1.88±0.13	1.13±0.29	64.0	$1.25^{0.59}_{-0.45}$	$6.8^{3.0}_{-1.9}$
1BIGBJ160618.4+134532	241.57667	13.75889	0.29	2.05±0.21	1.76±0.64	33.8	$1.65^{1.14}_{-0.77}$	$7.1^{4.7}_{-2.5}$
1BIGBJ161327.1-190835	243.36292	-19.14333	0.	2.14±0.15	3.15±0.82	34.1	$2.73^{1.25}_{-0.95}$	$10.5^{4.3}_{-2.7}$
1BIGBJ162115.1-003140	245.31333	-0.52778	>0.52	1.80±0.21	0.77±0.41	14.4	$0.93^{0.93}_{-0.58}$	$5.6^{4.7}_{-2.3}$
1BIGBJ162330.4+085724	245.87708	8.95667	0.533	1.91±0.20	1.23±0.52	35.5	$1.33^{1.05}_{-0.69}$	$7.0^{4.9}_{-2.5}$
1BIGBJ162646.0+630047	246.69167	63.01333	0.	1.91±0.17	1.00±0.33	51.6	$1.07^{0.65}_{-0.46}$	$5.5^{3.1}_{-1.8}$
1BIGBJ164220.2+221143	250.58458	22.19528	0.592	2.19±0.19	1.76±0.55	32.1	$1.46^{0.83}_{-0.60}$	$5.3^{2.8}_{-1.6}$
1BIGBJ164419.9+454644	251.08333	45.77889	0.225	1.65±0.16	0.48±0.20	39.1	$0.70^{0.56}_{-0.37}$	$5.4^{3.5}_{-2.0}$
1BIGBJ165517.8-224045	253.82458	-22.67917	0.	1.99±0.21	1.64±0.75	17.4	$1.64^{1.38}_{-0.91}$	$7.7^{5.6}_{-2.8}$
1BIGBJ171108.5+024403	257.78583	2.73444	0.	1.83±0.18	0.93±0.42	18.3	$1.09^{0.89}_{-0.60}$	$6.4^{4.2}_{-2.3}$
1BIGBJ174419.7+185218	266.0825	18.87167	0.	1.58±0.21	0.41±0.26	15.5	$0.65^{0.85}_{-0.48}$	$5.7^{5.6}_{-2.6}$
1BIGBJ174702.5+493800	266.76042	49.63361	0.46?	2.27±0.22	1.74±0.49	37.3	$1.37^{0.75}_{-0.53}$	$4.5^{2.6}_{-1.4}$
1BIGBJ184822.4+653656	282.09375	65.61583	0.364	1.59±0.15	0.50±0.21	52.8	$0.79^{0.63}_{-0.42}$	$6.8^{4.2}_{-2.4}$
1BIGBJ185023.9+263153	282.6	26.53139	0.	1.63±0.13	1.20±0.45	88.6	$1.80^{1.18}_{-0.85}$	$14.5^{7.1}_{-4.5}$
1BIGBJ185813.3+432451	284.55583	43.41417	0.	2.12±0.16	1.89±0.48	43.3	$1.67^{0.77}_{-0.58}$	$6.6^{2.9}_{-1.8}$
1BIGBJ193412.7-241919	293.55292	-24.32222	0.	1.60±0.12	0.88±0.30	53.5	$1.36^{0.81}_{-0.59}$	$11.5^{5.2}_{-3.4}$
1BIGBJ194356.2+211821	295.98417	21.30611	0.	1.44±0.08	2.01±0.57	194.7	$3.93^{1.84}_{-1.44}$	$42.9^{13.2}_{-9.8}$
1BIGBJ200204.0-573644	300.51708	-57.6125	0.	2.08±0.10	2.93±0.49	105.5	$2.69^{0.78}_{-0.64}$	$11.2^{3.0}_{-2.2}$
1BIGBJ201200.9-771219	303.00375	-77.20528	0.	2.10±0.30	0.78±0.52	9.8	$0.71^{0.89}_{-0.52}$	$2.8^{3.0}_{-1.2}$
1BIGBJ205242.4+081040	313.17708	8.17778	0.	1.51±0.23	0.25±0.20	15.3	$0.45^{0.73}_{-0.37}$	$4.3^{5.1}_{-2.2}$
1BIGBJ214533.3-043438	326.38875	-4.5775	0.069	2.64±0.31	1.34±0.47	9.7	$0.82^{0.55}_{-0.37}$	$1.9^{1.2}_{-0.6}$
1BIGBJ215214.0-120540	328.05875	-12.09472	0.121	2.26±0.14	3.77±0.76	81.3	$2.98^{1.06}_{-0.84}$	$10.0^{3.3}_{-2.2}$
1BIGBJ220107.3-590639	330.28042	-59.11111	0.	1.93±0.18	0.78±0.28	21.3	$0.82^{0.55}_{-0.38}$	$4.1^{2.4}_{-1.4}$
1BIGBJ220155.8-170700	330.4825	-17.11667	0.169	1.32±0.37	0.16±0.22	33.5	$0.38^{1.63}_{-0.47}$	$5.1^{14.1}_{-3.5}$
1BIGBJ221029.5+362159	332.62333	36.36639	0.	2.17±0.32	1.19±0.75	13.3	$1.01^{1.23}_{-0.72}$	$3.7^{4.1}_{-1.6}$
1BIGBJ221108.2-000302	332.78458	-0.05056	0.326	1.84±0.14	1.43±0.47	48.7	$1.67^{0.98}_{-0.71}$	$9.7^{4.8}_{-2.9}$
1BIGBJ223301.0+133601	338.25458	13.60028	0.214	1.51±0.24	0.24±0.19	15.4	$0.43^{0.73}_{-0.37}$	$4.2^{5.1}_{-2.1}$
1BIGBJ223626.2+370713	339.10958	37.12028	0.	1.85±0.20	0.98±0.48	29.1	$1.12^{1.01}_{-0.66}$	$6.3^{4.8}_{-2.4}$
1BIGBJ224910.6-130002	342.29458	-13.00056	>0.5	2.33±0.01	87.01±1.43	11240.5	$64.8^{1.93}_{-1.88}$	$202.8^{6.2}_{-6.0}$
1BIGBJ225147.5-320611	342.94792	-32.10333	0.246	2.07±0.19	1.60±0.51	48.6	$1.48^{0.90}_{-0.63}$	$6.2^{3.7}_{-2.0}$
1BIGBJ225613.3-330338	344.05542	-33.06056	0.243	2.56±0.21	2.23±0.42	39.7	$1.42^{0.54}_{-0.41}$	$3.6^{1.4}_{-0.8}$
1BIGBJ230634.9-110347	346.64583	-11.06333	0.	1.69±0.21	0.62±0.34	28.5	$0.86^{0.94}_{-0.56}$	$6.3^{5.7}_{-2.7}$
1BIGBJ232039.7-630918	350.16583	-63.155	0.2	1.84±0.16	0.84±0.30	43.6	$0.98^{0.64}_{-0.45}$	$5.7^{3.2}_{-1.8}$
1BIGBJ233112.8-030129	352.80375	-3.025	0.	2.05±0.15	1.95±0.54	40.8	$1.84^{0.90}_{-0.67}$	$7.9^{3.5}_{-2.2}$
1BIGBJ235320.9-145856	358.3375	-14.9825	0.	1.83±0.28	0.55±0.37	13.3	$0.65^{0.92}_{-0.49}$	$3.8^{4.9}_{-1.9}$

This paper has been typeset from a TEX/LATEX file prepared by the author.